SUPPLEMENTARY INFORMATION

Photoinduced Multi-Directional Deformation of Azobenzene Molecular Crystals

Yunhui Hao,[a] Shuai Huang,[b] Yanmei Guo,[a] Lina Zhou,[a] Hongxun Hao,[a] Christopher J. Barrett [c] and Haifeng Yu*[b]*

Table of Contents

1. Experimental Section

1.1 Materials and Equipment

4-Aminobenzonitrile and n-amyl bromide (Br-C_5H_{11}) were purchased from Tianjin Yuxiang Technology Co., Ltd. Hydrochloric acid (HCl), sodium nitrite ($NaNO_2$), phenol, sodium acetate (CH_3COONa), ammonia water ($NH_3 \cdot H_2O$), potassium carbonate (K_2CO_3) and N,N-dimethylformide (DMF) were purchased from Tianjin Jiangtian Chemical Co., Ltd.

^{1}H NMR spectra were recorded on a Bruker 500MHz spectrometer to confirm the molecular structure of the synthesized compounds. All spectra were collected in chloroform-d ($CDCl_3$) solution. The light sources for photoirradiation were a Height-LED HTLD-4 UV-LED light source (UV-light, 365 nm). UV-vis absorption spectroscopy of solutions and microcrystals were carried out on a UV-3010 spectrophotometer (HITACHI, Japan) with a 1 cm path length cell. A 785 nm Raman RXN2HYBRID analyzer from Kaiser Optical Systems, Inc. (Ann Arbor, MI) with iC Raman software was used to collect the Raman data. Thermal properties were determined by DSC analysis (Model name, Mettler Toledo, Co., Switzerland), with heating and cooling rates of 10 °C/min. A hot stage polarized optical microscopy system (HSPOM, Olympus BX51, Olympus Corporation, Tokyo, Japan) equipped with liquid nitrogen refrigeration system was used to observe the photoinduced multi-motions of crystals. Time-lapse images were acquired using a sensitive Kodak digital camera model name at a fixed time interval. Atomic force microscopy (AFM) was obtained by one scanning probe microscope in tapping mode (Nanoscope V, Bruker Co., Ltd). Powder X-ray diffraction (PXRD) was performed on a Rigaku D/MAX 2500 with a scintillation counter.

1.2 Syntheses

The azobenzene compound was synthesized according to our previously reported method.[1] The chemical reaction is shown in Scheme S1, and the ^{1}H NMR spectrum was recorded in $CDCl_3$ solution, as shown in Fig. S1.

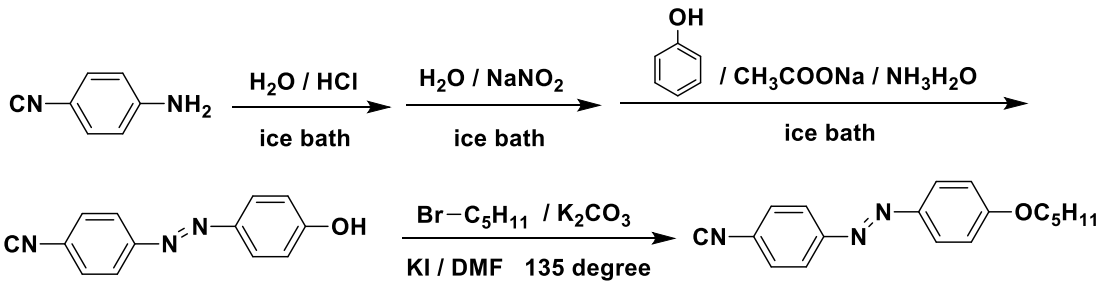

Scheme S1. Synthesis of the photoactive azobenzene compound.

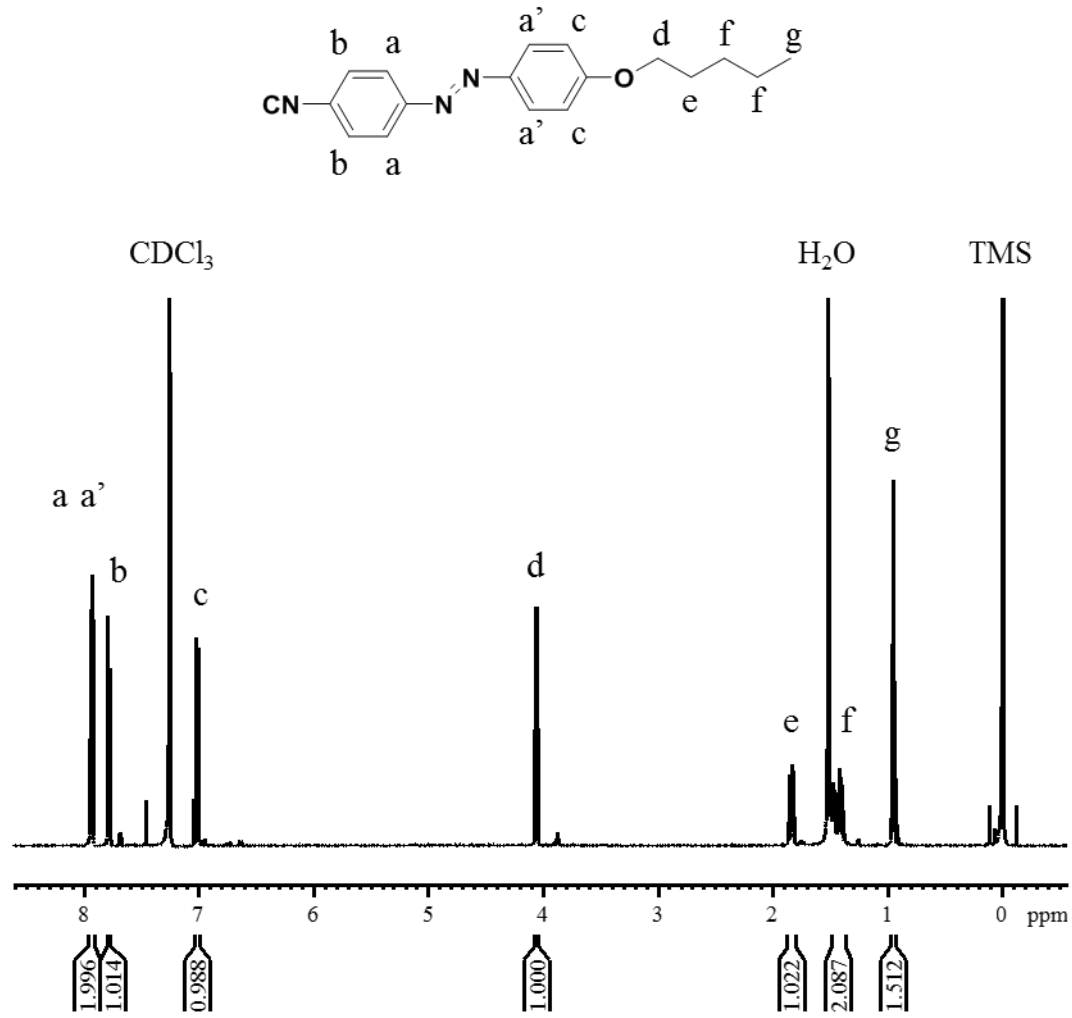

Fig. S1. ^{1}H NMR spectrum of the azobenzene compound (500MHz, $CDCl_3$, 25°C, TMS): δ 7.92-7.94 (4H, d), δ 7.77-7.79 (2H, d), δ 7.00-7.02 (2H, d), δ 4.04-4.07 (2H, t), δ 1.81-1.86 (2H, m), δ 1.37-1.49 (4H, m), δ 0.94-0.97 (3H, t). The peak at 1.53 ppm is due to water and the peak at 7.25 ppm is due to $CDCl_3$.

1.3 Preparation of ***trans-***AZ crystals

The plate-like ***trans-***AZ crystals were prepared by the floating-drop method.[2] To start, an excess amount of the azobenzene compound and toluene were added into a jacketed glass vessel and agitated by a magnetic stirrer at 300 rpm for about 2 h to reach solid-liquid equilibrium. The temperature was kept at 20 °C by a thermostat (Julabo CF41, Germany). Then, the agitation was stopped and the solution was kept still for 1 h to ensure the separation of liquid and solid. Then, the upper clear solution was withdrawn, filtered through a pre-heated 0.22 μm syringe filter and slowly dropped to the surface of triple deionized water in a petri dish (60×15 mm). The petri dish was covered and put into the vacuum oven for 24 h. Meanwhile, the temperature of the system was kept at 20 °C for slow evaporation. Finally, the ***trans-***AZ crystallized out as plate-like.

2. Characterization

2.1 Single Crystal X-ray Diffraction (SXRD)

The ***trans*-**AZ single crystal was cultivated by slow evaporation of the solvent of the ethyl acetate solution. Its PXRD shows a good consistency with above plate-like ***trans*-**AZ crystals (Fig. S2). A data summary is presented in Table S1.

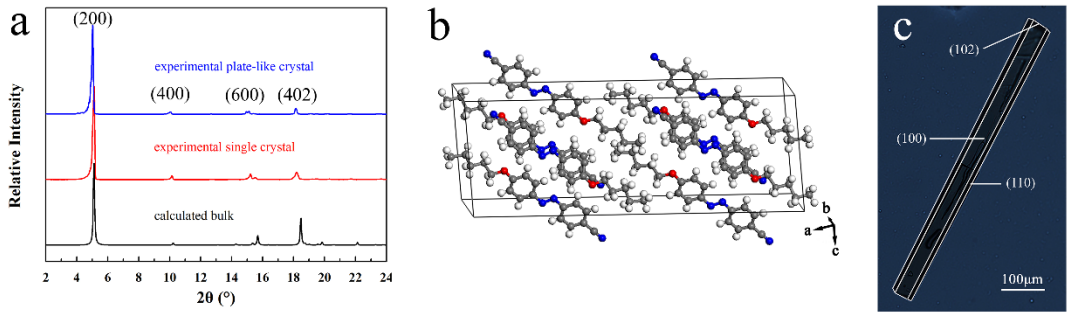

Fig. S2. (a) PXRD patterns of ***trans*-**AZ crystals show four sharp peaks, which were assigned to the (200), (400), (600) and (402) crystal surfaces based on crystallographic data. (b) Unit cells of ***trans*-**AZ azobenzene in stereo view. (c) Face indexing of crystal of ***trans*-**AZ.

Table S1. X-ray crystallographic data of ***trans-***AZ crystals.

Empirical formula	$C_{18}H_{19}N_3O$	
Formula weight	293.36	
Color of crystal	Orangered	
Temperature	113(2) K	
Wavelength	0.71073 Å	
Crystal system	Monoclinic	
Space group	P2(1)/c	
Unit cell dimensions	a = 34.80(2) Å	
	b = 7.32 (2) Å	α = 90°
	c = 12.47(2) Å	β = 96.17 (2) °
Volume	3159(5) $Å^3$	γ = 90°
Z	8	
Calculated density	1.234 Mg/m^3	
Absorption coefficient	0.079 mm^{-1}	
F (000)	1248	
Crystal size	0.20 x 0.18 x 0.12 mm^3	
Theta range for data collection	3.02 to 25.01°	
Limiting indices	-41<=h<=41, -8<=k<=8, -13<=l<=14	
Reflections collected / unique	18364 / 5341 [R(int) = 0.0398]	
Completeness to theta = 25.01°	95.8 %	
Absorption correction	Semi-empirical from equivalents	
Max. and min. transmission	0.9906 and 0.9845	
Refinement method	Full-matrix least-squares on F^2	
Data / restraints / parameters	5341 / 164 / 435	
Goodness-of-fit on F^2	1.035	
Final R indices [I > 2sigma(I)]	R1 = 0.0802, wR2 = 0.2096	
R indices (all data)	R1 = 0.1426, wR2 = 0.2635	
Largest diff. peak and hole	0.704 and -0.281 e.$Å^{-3}$	

2.2 UV-Vis absorption spectra of the AZ compound in THF solution

Photoisomerization of the AZ compound in THF solution was investigated by UV-Vis absorption spectroscopy. It can be seen that the maximum absorption peak initially remained constant at 365 nm and then shifted to 316 nm and 445 nm as the intensity of UV light (365 nm) and irradiation time was increased (Fig. S3a and c), corresponding to (n→π*) and (π→π*) excitation, respectively. After UV irradiation was turned off, the ***cis-***AZ solution was kept at different temperatures in the dark for 30 min and then its absorption spectrum was measured. It can be clearly seen that the recovery rate increased with temperature rising (as shown in Fig. S3d). Thus, the intensity of UV light, irradiation time and temperature are three major factors that will affect the photoisomerization reaction.

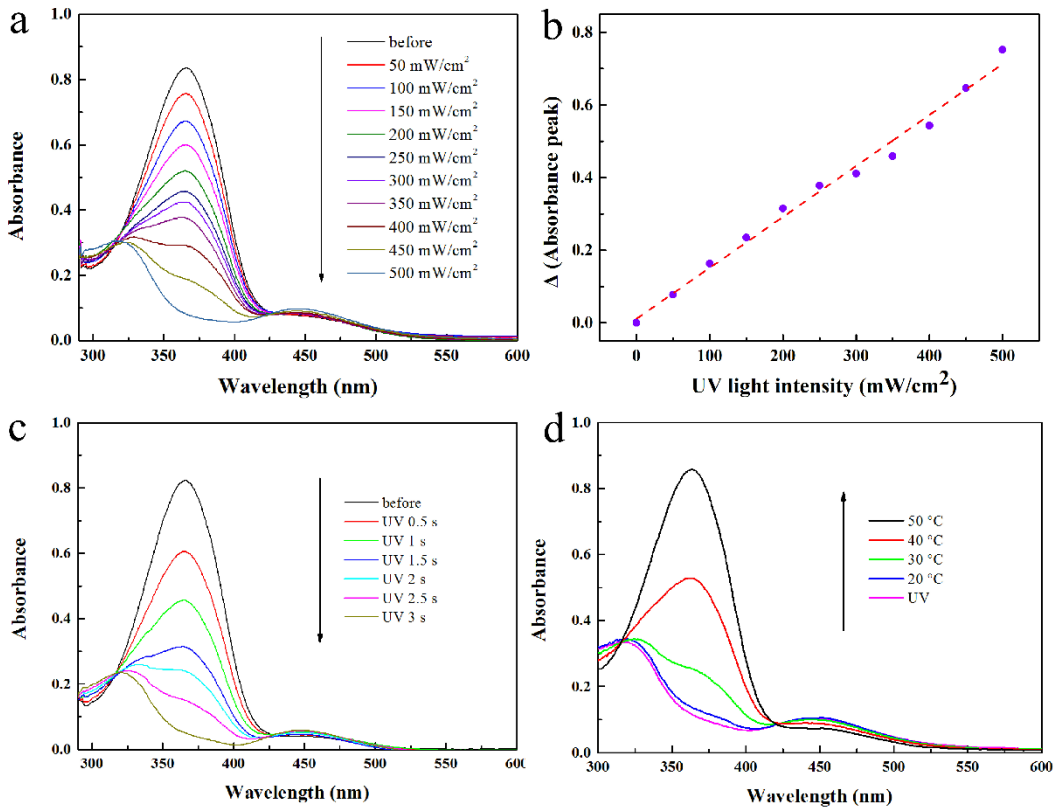

Fig. S3. Absorption spectral changes of the ***trans-***AZ (0.05mM) in THF upon (a) 3 s photoirradiation of UV light, and (b) its change of the absorbance peak at 365 nm as a linear function of the light intensity. Absorption spectral changes of the azobenzene with (c) UV irradiation time (500 mW cm^{-2}), and (d) the recovering process at different temperatures in THF solution. The wavelength of UV light is 365 nm.

2.3 Raman spectra of ***trans-***AZ crystals

The reversible photoisomerization behavior of the obtained AZ crystals was characterized by Raman spectroscopy. Generally, the ***trans-***isomer has strong stretching vibrations since its molecular structure is planar, while the ***cis-***isomer exhibits obvious torsional vibration since ***cis-***molecules have a dihedral angle.[3] These differences can be used to monitor the compositional changes between isomers.

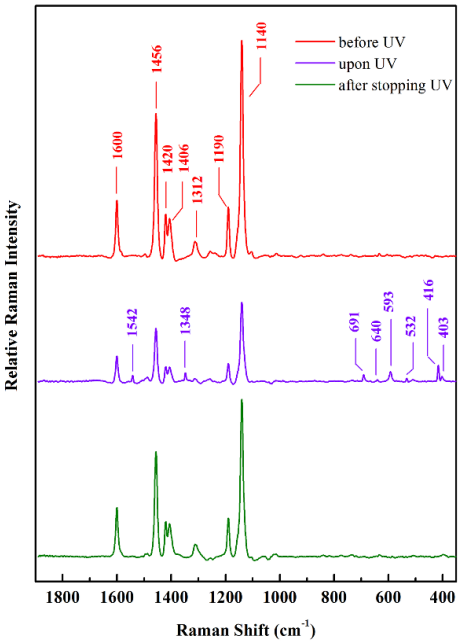

Summary of Raman Shift for type of vibration in AZ

Vibration[a]	Raman Shift (cm^{-1})	
	trans-	***cis-***
ν (NN)	1600	
	1452	1542
	1419	1348
	1402	
δ(NCC)	1312	1312
δ(CCH)[b]	1312	1312
ν (CN)	1191	1191
	1139	1139
τ (CNNC)	-	691
		640
τ (CCCH)[b]	-	592
τ (NNCC)	-	532
τ (CCNN)	-	416
		403

[a] ***ν*** = stretch, ***δ*** = deformation and ***τ*** = torsion.
[b] ***δ***(CCH) and ***τ*** (CCCH) is the motion within the phenyl rings

Fig. S4. Raman spectral changes of a suspension of plate-like crystals in ethane diol (the ethane diol solvent peaks were subtracted).

Before UV irradiation, the most notable features of Raman spectrum of ***trans-***AZ occurred at two ranges of bands (red line), 1600, 1456, 1420 and 1406 cm^{-1} corresponding to N=N stretching vibrations, 1312 cm^{-1} representing the phenyl rings deformation vibrations of NCC and CCH, and 1190, 1140 cm^{-1} attributing to C-N stretching vibrations. After UV irradiation for 3 min, several new torsional vibrations peaks appeared (blue line), such as the most intense peaks at 691 and 640 cm^{-1} (C-N=N-C torsion), 592 cm^{-1} (CCCH torsion within the phenyl rings), 532 cm^{-1} (N=N-C-C torsion), 416 and 403 cm^{-1} (C-C-N=N torsion). This could be explained by the appearance of the ***cis-***AZ isomer, which is caused by the transformation of planar molecules into steric molecules. The band assignments of ***cis-***AZ and ***trans-***AZ in table reveal several interesting vibrational shifts. For example, the intensity of peaks at 1600, 1456, 1420 and 1406 cm^{-1} representing N=N stretching vibrations decreased after UV irradiation, whereas new strong peaks at 1542 and 1348 cm^{-1} appeared. The C-N stretch represented by peaks at 1190 and 1140 cm^{-1} also decreased after UV irradiation. After 365 nm UV irradiation was stopped for 3 min, the Raman spectrum of sample almost recovered to its initial shape (green line).

2.4 Thermal properties

As shown in Fig. S5a, the melting point of ***trans***-AZ (MPTA) was observed at 108 °C in its DSC curve.

To evaluate the melting point of ***cis***-AZ (MPCA) crystals used in the experiment, the phase transition was *in-situ* observed by using hot stage microscope upon UV irradiation. As shown in Fig. S5d, a thick plate-like ***trans***-AZ crystal was first put on the hot stage. Then, it was heated from 25 °C with heating rate of 20 °C/min. During the whole experiment, the crystal was constantly irradiated with 365 nm UV light (from the bottom left side of the pictures in Fig. S5e). When the crystal was heated to 82.7 °C, the liquid state molecules flowed away and the crystal structure was destroyed. Then, the temperature was maintained constantly and the crystal gradually returned to its crystalline state after stopping UV illumination. This melting phenomenon indicated that the ***trans***-to-***cis*** photoisomerization has occurred on the upper crystal surface, and the approximate range of MPCA was determined.

Based on the above experimental results, the crystals were kept at 80 °C and exposed to 365 nm UV light for 2 min, and then quenched in liquid nitrogen (***sample-1***). As shown in Fig. S5b, a new gentle endothermic peak appeared at 74-83 °C, which is assigned as MPCA. In addition, compared with ***trans***-AZ crystals, the PXRD pattern of ***sample-1*** exhibited new Bragg peaks at 2θ ≈ 6.040 °, 12.255 °, and 18.479 °. These new peaks originate from the fully photoisomerized ***cis***-AZ crystallized from the photoinduced melt phase.

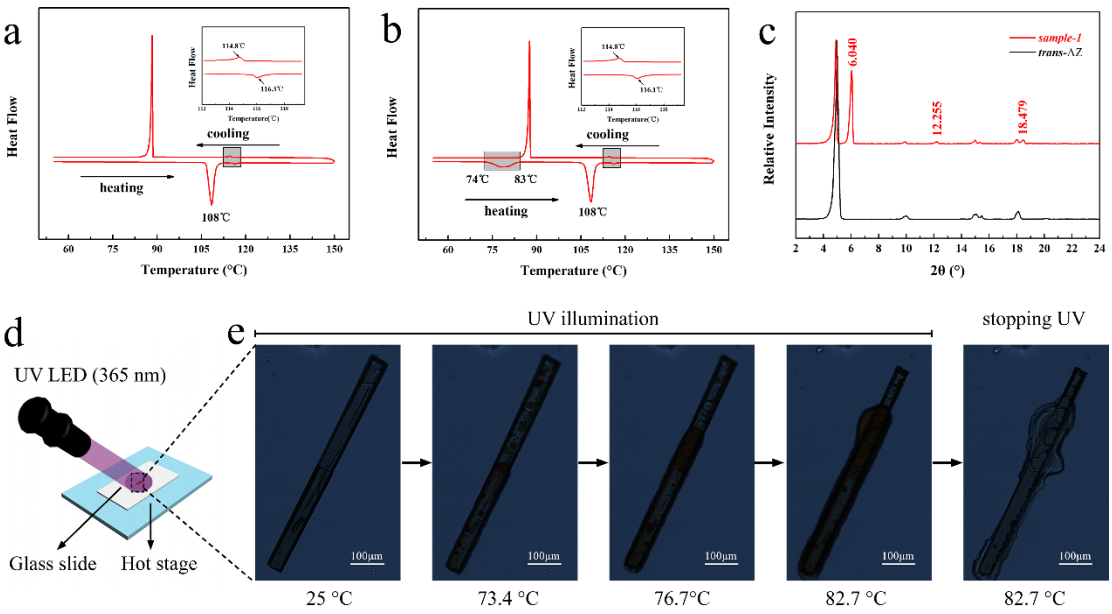

Fig. S5. DSC curves of plate-like ***trans***-AZ crystals: (a) before irradiation, and (b) kept at 80 °C by a hot stage and exposed under 365 nm irradiation for 2 min, then quenched in liquid nitrogen (***sample-1***). (c) PXRD patterns of ***trans***-AZ crystals and ***sample-1***. (d) Schematic illustration of the experimental setup for phase transition observation. And (e) images of phase transition of a thick plate-like ***trans***-AZ crystal.

3. Motion 1: Reversible Bending away from the Light Source

3.1 Factors influencing the bending motion

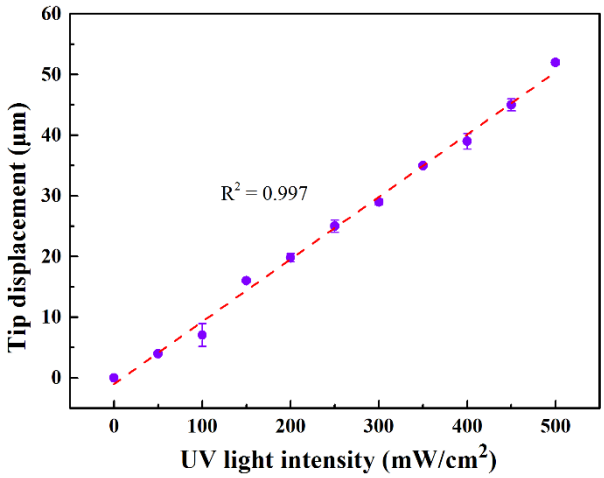

Fig. S6. Effect of UV light intensity on the tip displacement of the plate-like ***trans***-AZ crystal. The error bars give the standard deviation over five separate measurements.

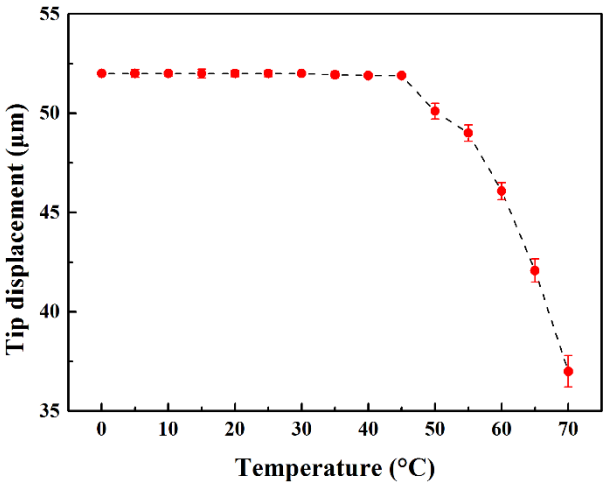

Fig. S7. Effect of temperature on the tip displacement of the plate-like ***trans***-AZ crystal. The error bars give the standard deviation over five separate measurements.

3.2 Summary of the PXRD parametric variations of the crystal faces

Table S2. Summary of the PXRD parametric variations of the crystal faces.

(200) plane	2θ(°)	d (Å)	Height	Area	FWHM
before	4.820	18.3175	32647	267279	0.139
UV	4.980	17.7296	23655	369872	0.259
after	4.821	18.3141	33176	271327	0.139

(400) plane	2θ(°)	d (Å)	Height	Area	FWHM
before	9.895	8.9638	896	8525	0.162
UV	10.020	8.8202	418	8827	0.359
after	9.860	8.9633	829	7840	0.161

(600) plane	2θ(°)	d (Å)	Height	Area	FWHM
before	14.919	5.9333	978	14180	0.246
UV	15.021	5.8933	637	16461	0.439
after	14.919	5.9333	897	12558	0.238

(402) plane	2θ(°)	d (Å)	Height	Area	FWHM
before	17.958	4.9353	2199	17432	0.135
UV	18.119	4.8920	1059	16765	0.269
after	17.997	4.9248	813	6720	0.141

4. Motion 2: Incomplete Reversible Bending towards the Light Source

4.1 Effect of temperature on bending motion

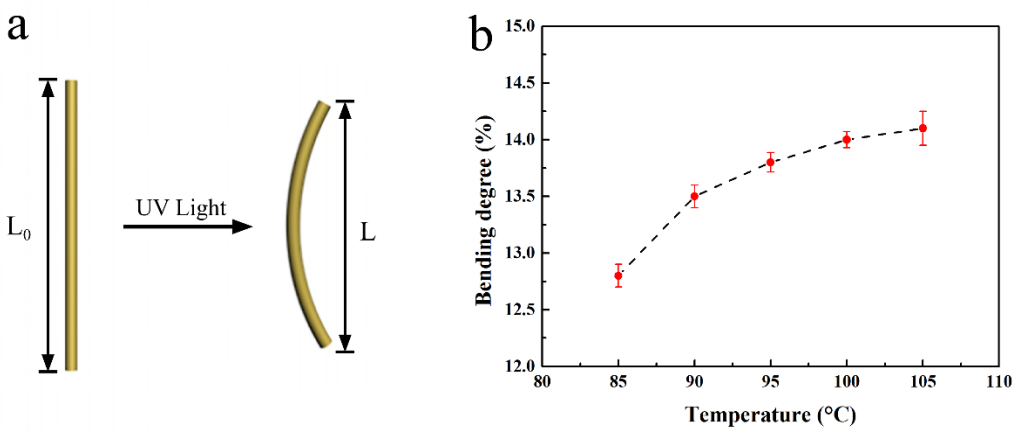

Fig. S8. (a) Schematic illustration of the bending degree of photomechanical crystals. (b) Dependence of ambient temperature on the bending degree of the plate-like ***trans-***AZ crystal. The experiment was carried out at the same photoirradiation condition (365 nm, 100 $mWcm^{-2}$, 15 s). The error bars give the standard deviation over three separate measurements.

4.2 Variable-temperature PXRD

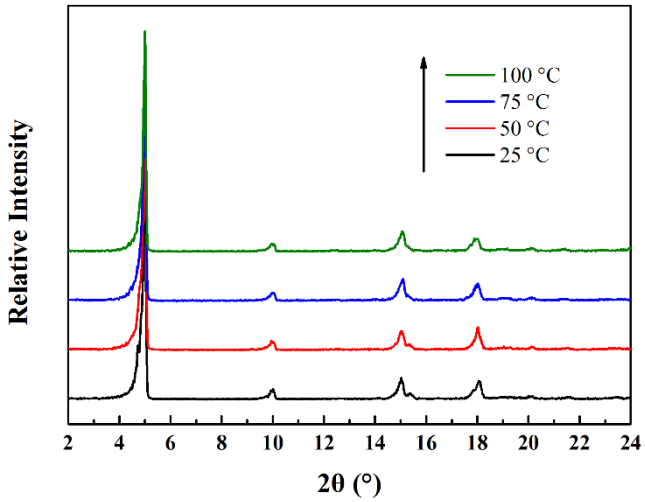

Fig. S9. PXRD patterns of ***trans-***AZ crystals as a function of temperature between 25 and 100 °C.

5. Motion 3: Bidirectional Bending Motion upon Photoirradiation

5.1 Crystal thickness dependence of the photoinduced bidirectional bending

The reaction depth of photoisomerization from the crystal surface (h_2) plays a very important role in the crystal bending behavior, because the ratio of h_2 to the crystal thickness is changed.[4]

Here, we investigated the influence the crystal thickness on the photoinduced bidirectional bending behaviors at 70 °C (near but below the MPCA). Fig. S10 shows the photoinduced bending of different thickness crystals before (0 s) and after UV light irradiation (1, 3, and 5 s) to the (200) face from the left. When the crystal thickness is 8.1 μm, the crystal cannot bend but melt gradually (Fig. S10a). The reason is that UV light penetrates the crystal and photoisomerization of ***trans***-to-***cis*** can occur homogeneously throughout the entire crystal since the crystal thickness is very close to h_2. Then, with continuous UV irradiation, the temperature of the irradiated surface increases up to MPCA, causing the ***cis***-AZs to melt. Thus, the whole crystal melts gradually. When the crystal thickness is 17.4 μm, the crystal demonstrates bidirectional bending motion (Fig. S10b which was copied from Fig. 7). In contrast, when the crystal thickness is 30.9 μm, the crystal only bends toward the incident light (Fig. S10c). Since 30.9 μm is considerably larger than h_2, photoisomerization of ***trans***-to-***cis*** can only occurs at the crystal surface. That means that the photothermal effect cannot affect the deeper inside of the crystal and the other side of the irradiated surface cannot expand. Thus, the bidirectional bending motion is no longer observed.

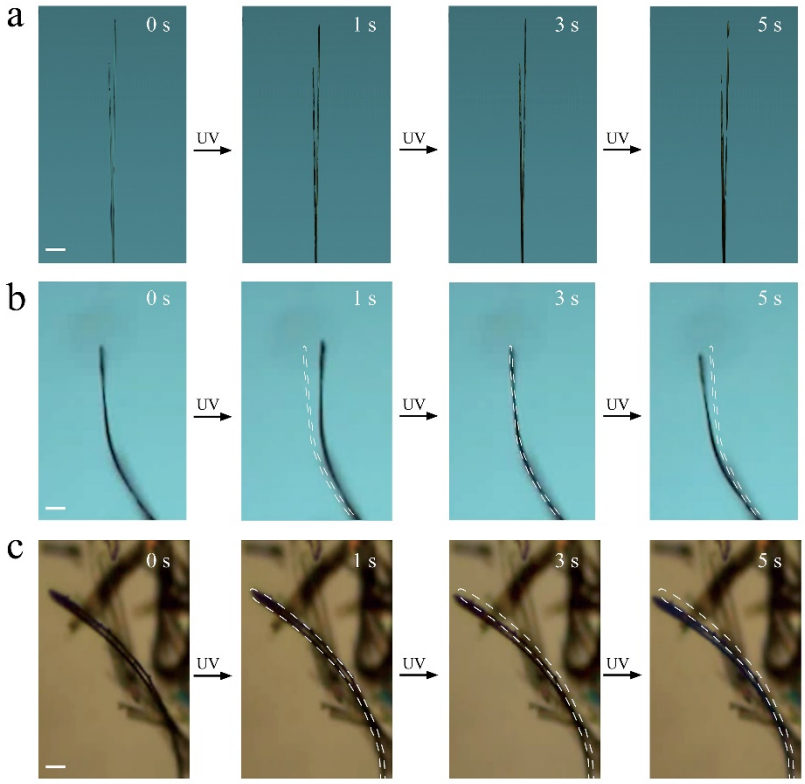

Fig. S10. Photoinduced bending behavior of ***trans-***AZ crystal upon UV irradiation from the left side at 70 °C in different thickness samples: (a) 8.1, (b) 17.4 and (c) 30.9 μm. The scale bar is 100 μm.

6. Supplementary movie legends

Movie S1-1. Photoinduced reversible bending motion backwards from the UV light of the plate-like crystals at 0 °C.

Movie S1-2. Photoinduced reversible bending motion backwards from the UV light of the narrow plate-like crystals at 0 °C.

Movie S2. Photoinduced incomplete reversible bending motion forwards from the UV light of the plate-like crystals at 85 °C.

Movie S3. Photoinduced bending motion which changes its direction of the plate-like crystals at 70 °C.

7. References

[1] Z. Cheng, T. Wang, X. Li, Y. Zhang and H. Yu, *ACS Appl. Mater. Interfaces*, 2015, **7**, 27494.

[2] M. Campione, R. Ruggerone, S. Tavazzi and M. Moret, *J. Mater. Chem*., 2005, 15, 2437.

[3] C. M. Stuart, R. R. Frontiera and R. A. Mathies, *J. Phys. Chem. A*, 2007, 111, 12072.

[4] D. Kitagawa, R. Tanaka and S. Kobatake, *Phys. Chem. Chem. Phys*., 2015, 17, 27300.